INTERNATIONAL BUILDING SIMULATION ASSOCIATION ENGLAND

Proceedings of BSO 2018:
4th Building Simulation and Optimization Conference, Cambridge, UK: 11-12 September 2018

Calculation Examples Using the NETS Simulation Program as a General-Purpose Network Model for Heat, Air, and Gas Movement in Buildings

Atsumasa Yoshiura, Hiroyasu Okuyama,
Mao Yamaguchi,Nanase Ishigaki, Ryunosuke Harada, Tatsuki Someya
Kanagawa University Department of Architecture Faculty of Engineering
Yokohama City, Japan

Abstract

The method of thermal response factors for walls is one of the main ways to calculate heating and cooling loads, but it runs into problems when considering, for example, the aeration layer in a wall. On the other hand, computational fluid dynamics is used to calculate the airflow and temperature distribution in indoor spaces, but it is ill suited for calculating the long-term thermal load of buildings. As an engineering model with few of the restrictions of these conventional models, the thermal and airflow network model has long been known. However, it refers to several distinct models in that the modeling concepts and computational theory vary from one researcher to another. In this paper, we introduce a certain type of network model, the calculation program NETS, and application examples.

Introduction

Placing all calculation objects in a spatial coordinate system does not necessarily produce a practical predictive model for calculating the movement of heat, air, or gases such as water vapor in buildings. Rather, it is necessary to simplify and idealize the actual objects and setting to produce an engineering model. One such model is a network model. We have developed a general-purpose computer program called NETS (Okuyama 1985,1987,1999,2002). Herein, we describe our network model and then introduce three calculation examples that utilize NETS features.

The first example is a so-called air-cycle house with aeration layers inside the walls. The results show that the air layers are more important for preventing condensation inside the walls than for saving energy.

The second example is a multi-story building that removes internal heat from a data center by the stack effect of natural ventilation. On each floor, outside air is introduced into an underfloor space, and the heat exhaust ducts extend for three stories along the outer wall from the ceiling space. We investigate the negative effect of the elevator shaft.

The third example is a sensible-heat-recovery ventilation system for a residential house. A fan that reverses the direction of airflow is attached to a ceramic cylinder with many honeycomb-like holes. Two cylinders are used for room ventilation. Alternating supply and exhaust is repeated in a 2 min cycle. Heat is stored when exhausting air and recovered when supplying air. This is simulated as a mode change in the airflow network. We performed laboratory experiments on this system and compared them with the NETS predictions.

A thermal/airflow network model

The terms "thermal network model" and "airflow network model" have been used for a long time. However, different researchers have used different modeling concepts and mathematical solution methods for these models. Herein, we provide one example of modeling and analysis methods. A thermal network comprises nodes with a generalized heat capacity $m_{i,j}$ connected by generalized thermal conductance $c_{i,j}$, where the subscripts i and j indicate the nodal numbers. The values of these parameters can be obtained by spatial discretization using the finite volume method (FVM) or finite element method (FEM). Generalized thermal conductance represents various forms of heat transfer by the same symbol $c_{i,j}$, as shown in *Figure* 1. The subscripts i and j also specify the address of each matrix element. The FVM gives only diagonal elements of $m_{i,i}$ but the Galerkin method in FEM also gives $m_{i,j}$ of non-diagonal elements. These concepts realize compatibility between FVM and FEM and integration of these models.

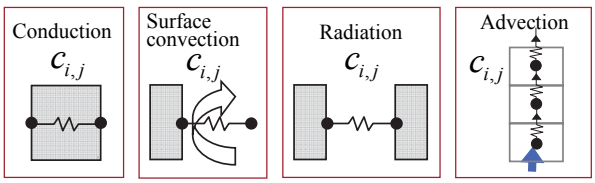

Fig.1: Generalized thermal conductance $c_{i,j}$.

The ordinary differential equation for the heat flow balance at each node assumes that the model is a fully connected and coupled system, with each node connected to all the other nodes as shown in *Figure* 2. The nodes that are actually connected have non-zero conductance, and the other connections are initially and automatically set to zero because of the default value of computational memory. These ideas allowed us to develop an equation and

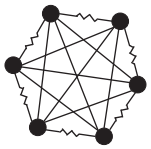

Fig.2: A fully coupled system of thermal network nodes.

algorithm that can be applied for any object figure and any spatial dimension.

We have deduced the exact solution of the system of simultaneous ordinary differential equations formed by the nodal equation using projective decomposition into eigenspaces. For practicality, however, we usually use the backward time difference method, for which unconditional stability has been proved mathematically.

The airflow network consists of zones such as room spaces and flow paths such as openings and ducts, as shown in *Figure* 3. A fan is attached to a flow path. The duct branches and mixing points are assumed to be zones with total pressures consisting of static and dynamic pressures. The zone pressure nodes at the height of the bottom of each zone have the static pressure as the total pressure. The essence of our general-purpose airflow network calculation program is the data structures and algorithms for calculating the airflow imbalance at each zone and constituting the Jacobian matrix of the partial derivatives. For this, the method of indirect addressing from assembly language is applied using the data arrays containing the zone numbers on both sides of each flow path.

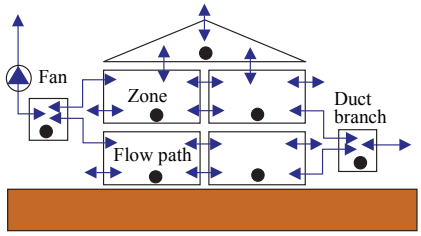

Fig.3: Airflow network model consisting of a total-pressure node system.

If we use the usual Newtonian method to solve for the zone pressure that balances the airflow in each zone, oscillations such as those shown in *Figure* 4 will often occur, making convergence difficult. Therefore, we use a modified Newtonian method in which only half of the calculated pressure corrections are applied in the iteration process approaching the solution.

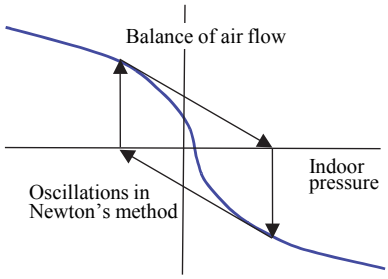

Fig.4: Oscillations in usual Newtonian method.

In situations involving natural ventilation due to indoor and outdoor temperature differences, both network models must be coupled. Each model can be regarded as a nodal system representing either temperature or zone pressure. In the final stage of the overall model construction, we define arrays containing node numbers that facilitate correspondence between the two systems. These arrays transform the node number from one system to the other. Through these arrays, the air densities due to the room temperatures are input to the airflow network, and the airflows are input to the thermal network as generalized thermal conductance.

The transfer of any type of gas including water vapor can be modeled in a similar model that excludes radiative heat transfer. The coupled effect of heat and moisture is remarkable in evaporative cooling. However, if we can refer to dynamic material properties of moisture transfer such as absorptivity, emissivity, and specific capacity, then we can also model the coupled transfer of heat and moisture in materials.

The coupled simulation of these three models is calculated with a delay of the time integration interval. For a steady-state solution, iterative calculation is performed using these three models. The switching between steady- and non-steady-state simulation is done simply by setting capacitance parameters such as $m_{i,j}$ to zero or non-zero, respectively, because the time integration scheme is unconditionally stable even for the zero-capacitance system.

A calculation program called NETS based on the above theory simulates heat, air, and vapor (gas) transfer in buildings, including thermal load, mode changes, and state feedback control calculations (e.g., PID and scheduled control). The user interface program of NETS was developed in the House Japan project (1994–2001), which was supported financially by the Ministry of International Trade and Industry.

Effect of ventilated double layers in the walls of wooden houses

Some housing companies have proposed methods of ventilation that rely on natural energy, with double air layers on both sides of an insulation layer inside a wall. These air layers are circulated or ventilated by taking advantage of solar heat or density differences caused by temperature differences between the indoor and outdoor environments. An air damper controls the airflow according to the season, and energy saving over conventional methods can be expected in heating and cooling. In one study, the energy saving effect was investigated by Lin (2015) using TRNSYS (2015). Here, we use NETS for simulation of heat, airflow, and water-vapor transfer. In addition, we investigate the risk of condensation inside the walls, which may cause decay of the wooden material and worsen health, for different ventilation methods.

Calculation model

A house with a width of 10 m, a depth of 7 m, and a height of 5 m was modeled using thermal, airflow, and vapor networks as shown in *Figure*s 5–7. The left-hand side of the cross section is facing south. The materials and thickness (unit: mm) of the roof from outdoor to indoor are slate (10), plywood (10), air layer (60), foamed styrene (50), plywood (10), air layer (60), and plasterboard (10), and for the wall they are tile (10), plywood (10), air layer (60), foamed styrene (50), plywood (10), air layer (60), and plasterboard (10).

We compared a situation in which wall ventilation and circulation occurred and a situation in which the air layer was closed using a damper. These changes can be

handled in NETS using the concept of mode changes. For appropriate predictions of the airflow in the wall, the gap is important as well as the intended slits at the top and bottom of the wall. For the equivalent leakage area of actual houses, we referenced the results of the investigation by Yoshino *et al*. (JIS-A2201, 2003). and used 5 cm^2/m^2 (unit floor area) as an average. The gap, whose actual location is uncertain, was distributed evenly around the outside wall to approach this value. Measurement for the air-tightness by computation yielded a value of 4.35 cm^2/m^2. The pressure-loss coefficient of the air layer was determined using a method normally used to design air ducts (SHASE-J 2010). The effect of the shape resistance due to flow compression, expansion, and bends was larger than the effect of the friction resistance.

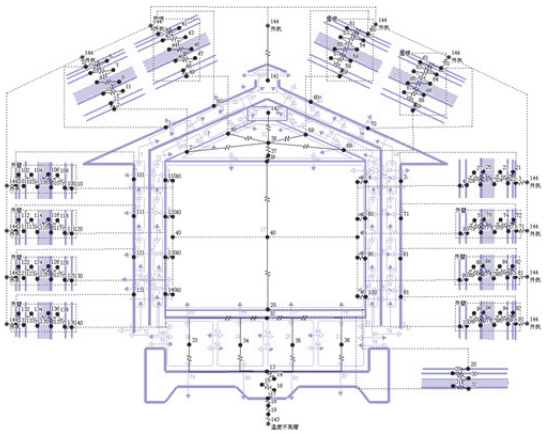

Fig.5: Thermal network model with underlying diagram of building section

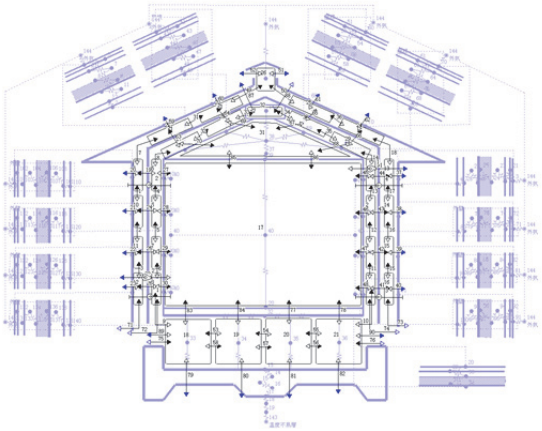

Fig.6: Airflow network model with underlying diagram of building section

Calculation conditions

The thermal-load calculation function provided by NETS was used to perform 24 h heating and cooling. The indoor temperature was set to 26°C during summer and 22°C during winter; the relative humidity was set to 50% in both cases. The supply of fresh air and exhaust of room air were both achieved using fans, and the air exchange rate was 0.75 1/h. The energy performance was investigated by calculating the sensible and latent-heat loads. We also investigated the condensation inside the walls using a coupled vapor network. The periods used for the investigation were August 8–14 for summer and February 8–14 for winter. These 7 d periods were preceded by a 7 d ramp-up period.

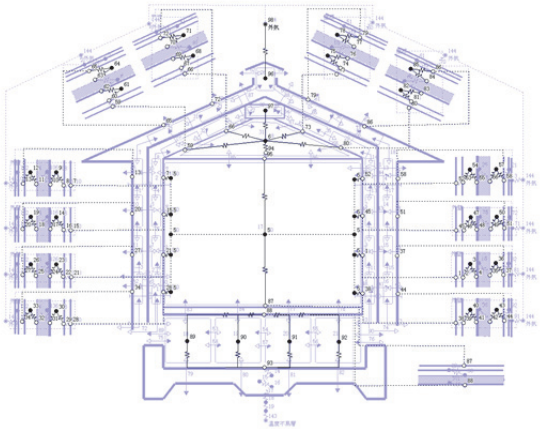

Fig.7: Water-vapor network model with underlying diagram of building section

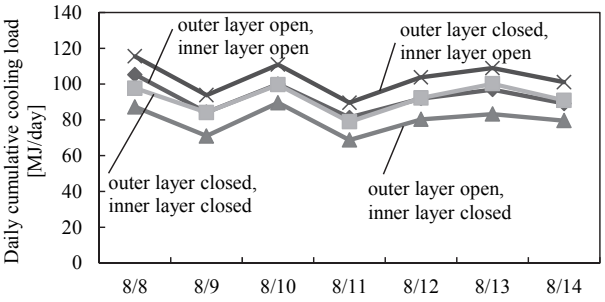

Fig.8: Cooling load according to whether ventilated double layers are open or closed

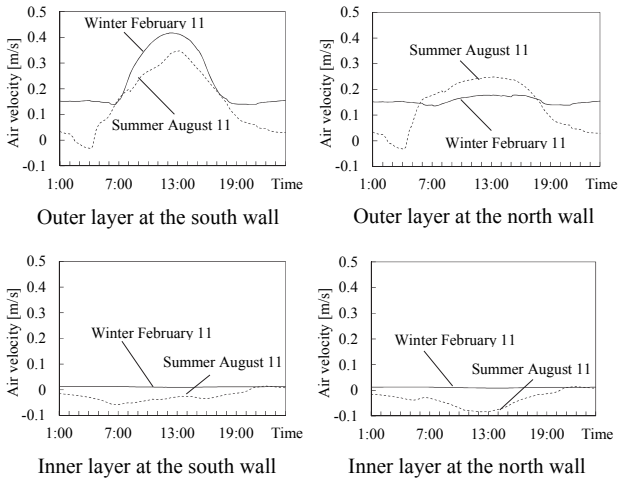

Fig.9: Air velocities inside walls

Summer results

We investigated four cases of open or closed dampers for the outer and inner air layers. The cooling load was lowest in the case in which the inner layer was closed and the outer layer was open, as shown in *Figure* 8. This is because the outer layer expels the heat from the solar

radiation absorbed on the exterior wall. By contrast, the cooling load was highest in the case in which the outer layer was closed and the inner layer was open. This is because the high-temperature outdoor air (OA) enters the inner layer. Therefore, it is best to close the inner layer and open the outer layer. *Figure* 9 shows the airflow velocity in the air layers of the south and north walls. On a typical summer day (August 8), upward velocities were generated in the outer layers of the south and north walls, while small downward velocities occurred in both inner layers.

Winter results

During winter, the heating load is naturally the smallest when the dampers for both air layers are closed, as shown in *Figure* 10. However, internal condensation occurs on the interior surface of the exterior material in the outer layer, as shown in *Figure* 11. However, opening the outer layer and letting OA infiltrate will expel the moisture and prevent condensation. Furthermore, the difference in the heating load is small between the outer air layer being open or closed.

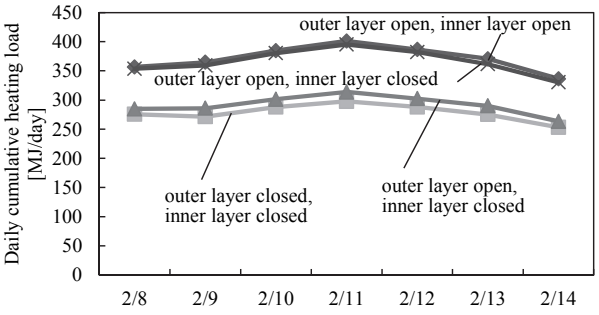

Fig.10: Heating load according to whether the air layers are open or closed.

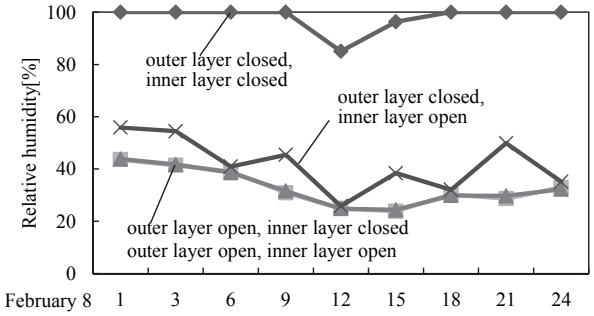

Fig.11: Condensation inside wall according to whether the air layers are open or closed.

Therefore, during the winter season, it is best to open the outer air layer and to close the inner layer, which is the same recommendation as for the summer season. The remarkable upward air velocities were generated by solar heat in the outer layer as shown in *Figure* 9, while the air of the inner layer hardly moved because the damper was closed. The investigation results described above for summer and winter imply that the inner air layer is unnecessary and that the outer air layer should always be left open. The outer air layer is useful for expelling the heat from solar radiation during summer and for expelling moisture from the interior and the structural materials of the walls, thereby preventing internal condensation and decay of wooden material. The outer aeration layer is rather necessary in case of using rock or glass wool insulation, because it is easy to dissipate the water vapor from indoor to outdoor, so that a healthy building environment can be obtained.

Influence of elevator shaft on natural-ventilation cooling of multi-story buildings

Because of the widespread adoption of the Internet in recent years, the number of data centers is increasing, and these require large amounts of energy-cooling in space caused by heat-generating equipment. Cooling utilizing natural ventilation based on the stack effect is a promising way to provide effective cooling to multi-story buildings. In the present paper, we investigate the adverse effect of vertical holes on natural ventilation. For this purpose, we extended the model by adding a tracer-gas-flow network model, making it possible to evaluate the effects of air movement separately from heat transmission through the exterior walls.

Calculation model

A sketch of the building is shown in *Figure* 12 and the thermal and airflow network models are shown in *Figure*s 13, 14 respectively. The floors of the server room occupy the lower six stories of the building. The third floor is modeled in detail with more zones than on the other floors, as shown in the diagram at the bottom of *Figure*s 13, 14. The exterior wall consists of four surfaces, one facing southeast, one southwest, one northwest, and one northeast. On each floor, OA enters the crawl space under the grating floor, and a heat exhaust duct with a height equivalent to three stories rises from the space above the grating ceiling. Therefore, the top three stories are designated for use as office space.

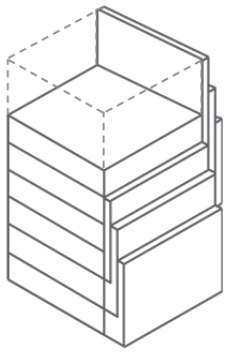

Fig.12: Sketch of the multi-story building with natural ventilation

A vertical hole was installed in the center of the building as an elevator shaft. Each story had a floor area of 400 m^2 (20m×20m), a floor height of 5.2m, slab and wall thicknesses of 0.2m and 0.15m, respectively, a space above the ceiling with a height of 1m, a ceiling height of 3m, a crawl space of 1m, a window area of 20m^2 with a glass thickness of 8mm, a shaft horizontal cross-sectional area of 9 m^2 (3m×3m), and a server heat generation of 80 kW. To evaluate the net cooling effect by the airflow,

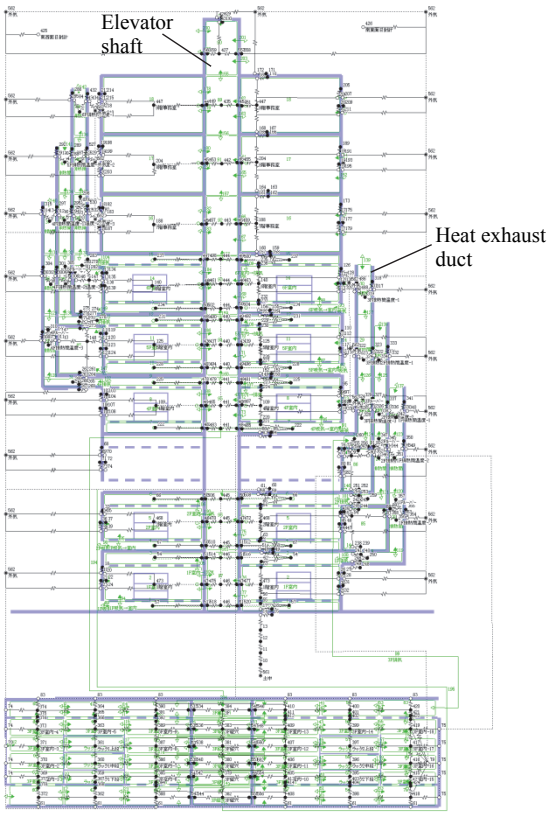

Fig.13: Thermal network model with underlying diagram of building section

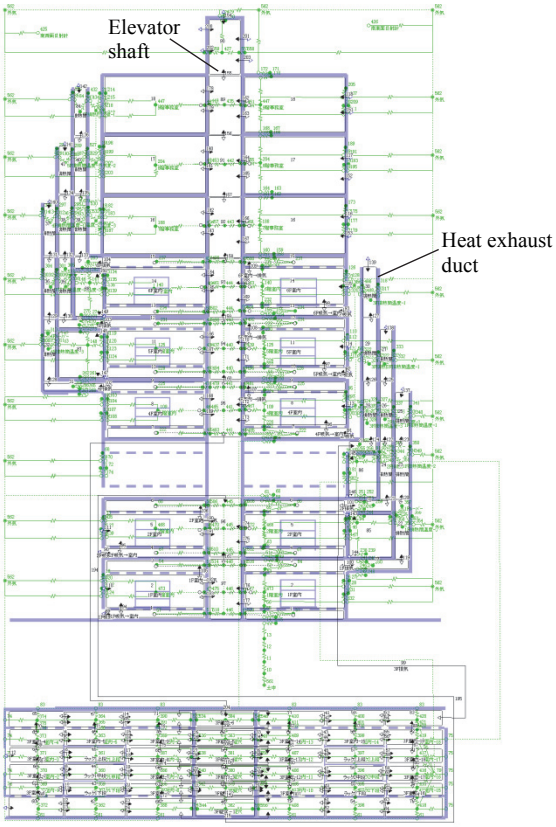

Fig.14: Airflow network model with underlying diagram of building section

we generated tracer gas for each story at a rate of 0.8 g/s, calculated the gas concentration, and evaluated the effective air exchange rate (AER). The intake and exhaust vents had a cross-sectional area of 20m^2 (20m × 1m).

The height of the prolonged heat exhaust ducts was 15 m, the same height as the three stories. The ducts were made of glass, and solar-radiation-heat-absorbing louvers of dimensions 20 m × 5 m were installed at the lower part of each exhaust duct to produce a solar stack effect.

We used the standard meteorological data of Tokyo for only the first four days in January. However, the OA temp was set constantly to 0°C. The calculation time interval was 5 min to obtain appropriate coupling among the heat, ventilation, and gas. The first three days were used as the ramp-up period, and the results for the fourth day were used in the investigation. To evaluate the solar-radiation effect on only the heat exhaust ducts, we set the solar absorptivity of the other walls to zero. The equivalent leakage area was set to 0.0045 m^2 based on the heuristic value of 5 cm^2 per unit area of the horizontal cross section of the shaft. Considering the situation in which the doors are open, we tried 10, 100, and 1,000 times the leakage size, making four models in total.

Calculation results

Comparison of effective air exchange rate and direct outdoor-air infiltration rate

The effective AER is evaluated as G/C, where G is the gas-generation flow rate and C is the gas concentration in the zone. This effective AER considers the effect of the OA via the neighboring zones. *Figure* 16 shows the effective AER for each floor for different equivalent leakage areas. The direct OA infiltration rate is evaluated by Q/V, where Q is the infiltration flow rate into the crawl space on each story and V is the volume of the zone. *Figure* 17 shows the direct OA infiltration rate for each story for different equivalent leakage areas. In the models with the leakage areas of 0.0045 m^2 and 0.045 m^2, both the effective AER and the direct OA infiltration rate remained the same for all stories. Concerning the effective AER and the direct OA infiltration rate, the ratios of the sixth floor to the first floor are 0.61 and 0.46, respectively. This means that infiltration via the elevator shaft contributes to the ventilation somewhat.

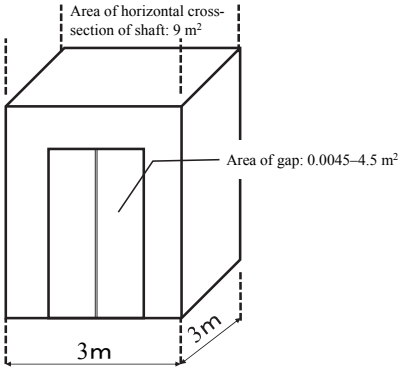

Fig.15: Sketch of the equivalent leakage area in elevator shaft.

Comparison of indoor–outdoor temperatures differences

Figure 18 shows a graph of the indoor and outdoor temperature difference of each floor according to the different air leakage area of the elevator shaft. In the models with a high degree of air-tightness of 0.0045 m^2 and 0.045 m^2, the indoor temperature was maintained approximately 3.8°C higher than the outdoor temperature for all stories. However, in the model with the leakage area of 4.5 m^2, there were deviations of 0.8°C lower for the first floor and 1.2°C higher for the sixth floor than the average of all stories. However, the indoor temperature of each server room was kept only about 5.0°C higher than the outdoor temperature.

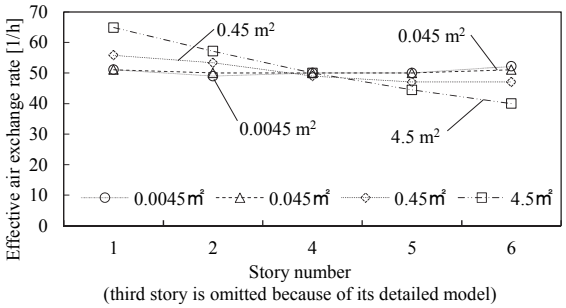

Fig.16: Effective air exchange rate (AER).

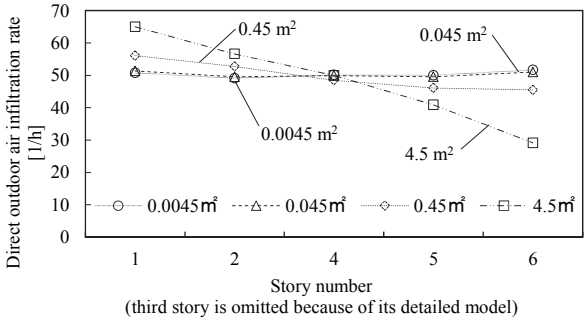

Fig.17: Direct outdoor air (OA) infiltration rate.

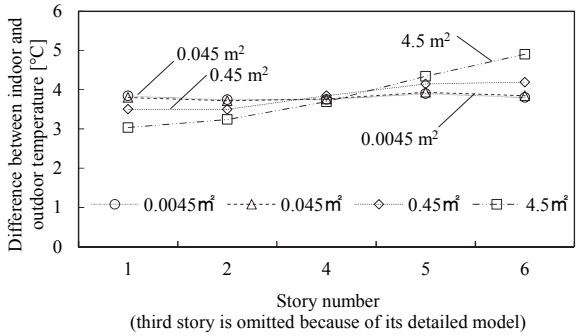

Fig.18:Differences between indoor and outdoor temperatures.

Heat-recovery ventilation equipment with alternating heat storage and release

Buildings are being constructed nowadays with higher levels of thermal insulation, and so it is becoming increasingly important to reduce the relative heat loss due to ventilation. An engineering thermal and ventilation model was constructed for a sensible heat-recovery ventilation system with alternating heat storage and release and investigated for its energy-saving performance. We also installed actual devices in a box that mimics a ventilation room. The box was placed in a laboratory at our university, and we used it to experimentally assess the validity of the calculation model.

Associated experiment

Figure 19 shows the box (a prefab refrigerator box) containing the sensible-heat recovery system with alternating heat storage and release that mimics the ventilation room. The device has a cylindrical ceramic element with a length of 150 mm and a diameter of 165 mm. Two devices were installed in the box. While one device is supplying air for 60 s, the other device is exhausting air for 60 s; in the next 60 s interval, the fan blowing direction is changed and switched between performing air supply and exhaust. The fan flow-rate deceleration and acceleration for 10 s is a part of the 60 s. This cycle is repeated with a period of 120 s. The system reduces the thermal load due to ventilation. We installed an electrical heater with an inside fan. We took measurements over a period of 3 h while the interior of the box was heated. We measured the temperatures of the air inside and outside the box, the supply air temperature, and the power consumption of the electric heater with a fan. We also measured the one-way intermittent supply and exhaust. *Figure* 20 shows where the temperatures of the supply and exhaust air were measured and the nodes in the calculation model that correspond to these points.

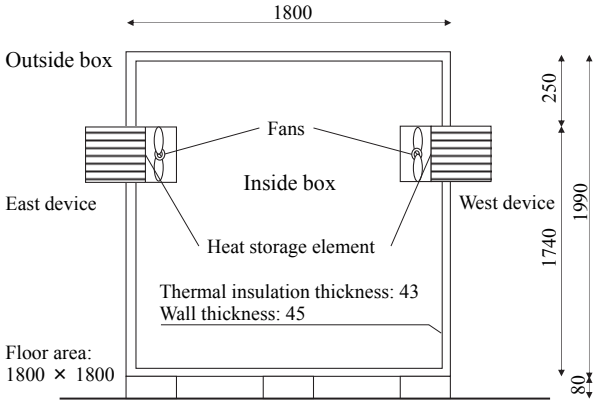

Fig.19: Experimental ventilation box constructed using a prefabricated refrigerator. (unit: mm)

Thermal and airflow network model

These models are shown in *Figures* 21 and 22, respectively. The heat storage cylinder has 31 sheets × 31 ceramic plates forming slender flow paths like honeycombs. The thermal properties of the ceramics are a conductivity of 2.1 W/mK, a specific heat of 0.91 kJ/kgK, and a density of 2.7 g/cm^3 (Deutinger 2013). The inner surface area of the honeycomb plate is 0.796 m^2. The plate thickness is 1 mm, and the outer thickness of the cylinder is 1.5 mm. The air passes through the cylinder and the temperature changes by

exchanging heat with the ceramic. This change was modeled by dividing into four segments along the flow direction; more segmentation was tried, but four was a suitable degree of segmentation. The airflow network model has the fan components at a fixed flow rate of 55 m^3/h or zero. Because we are in the early stage of our study, we disconnected the connections between the ventilation devices and the box wall model. We focused on the component performance model. We compared the experimental and computational results for the supply and exhaust air temperatures inside the box of two devices. The air temperatures measured inside and outside the box were used as inputs to the simulation model.

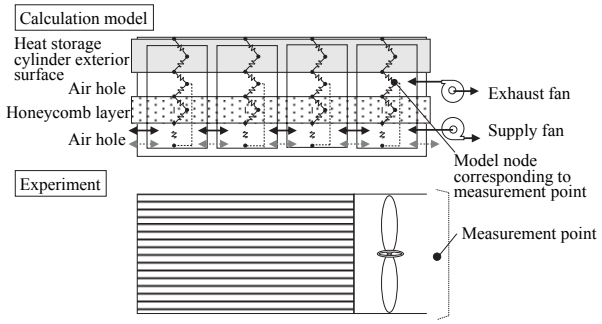

Fig.20: Points of supply and exhaust temperatures of measurements and corresponding nodes of thermal network.

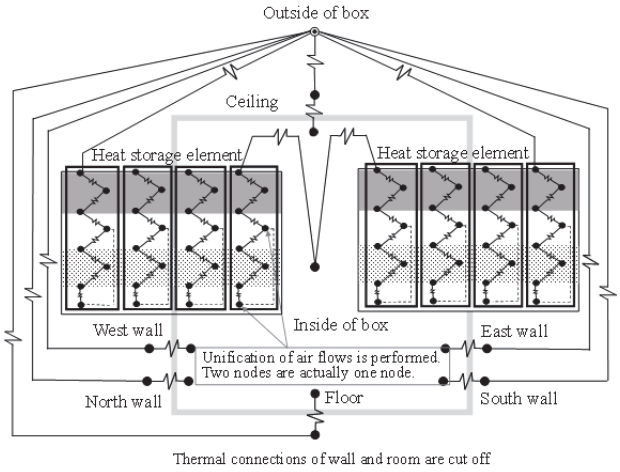

Fig.21: Thermal network model for heat recovery ventilation unit.

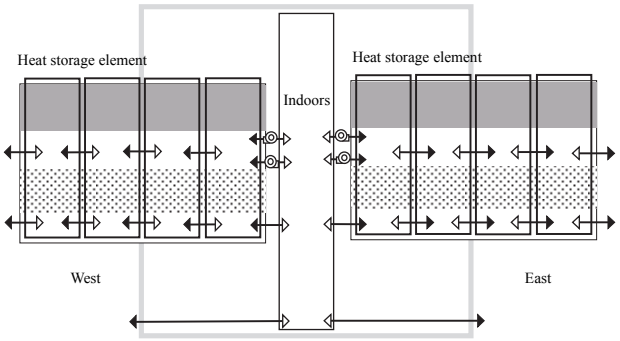

Fig.22: Airflow network model for the devices.

Comparison of measurements and prediction

The heat storage element consisted of a fine honeycomb structure, making it difficult to model the heat transfer of the actual shape. Therefore, the surface areas where the convective heat transfer takes place and the sectional areas through which conduction takes place were modified by the search method to make the calculation results approach the measured supply and exhaust air temperatures. We also corrected the nodal heat capacities from the specific heat in the product specification. *Figure* 23 shows that the experimental and computational results of the air supply and exhaust temperatures on the west device were in similar ranges of temperature variation. *Figure* 24 is a magnification of the final 10 min of the process in *Figure* 23. The predicted temperature remains slightly lower than that measured; some of the causes of this difference are thought to be a crude fan airflow-rate change of only two stages, a coarse time integration interval of 10 s, and insufficiency in the heat transfer model of the element. For these parametric optimizations, it may be possible to apply system identification theory (Okuyama 2012) but the state (temperature or gas concentration) of each node would have to be observable, and that is problematic. Incidentally, One segment along the cylindrical ceramic may be sufficient, by applying the solution of the first order differential equation, and more appropriate exit temp would be obtained.

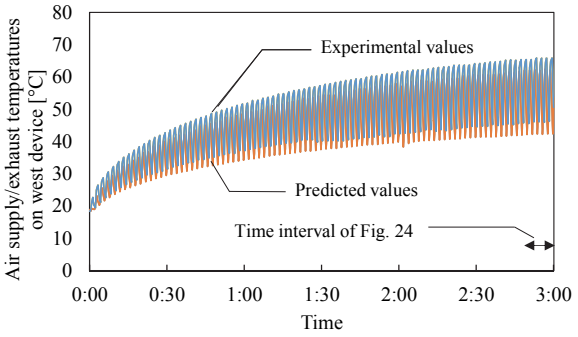

Fig.23: Air supply and exhaust temperatures on west device when heat capacity and areas of heat transfer and conduction are changed.

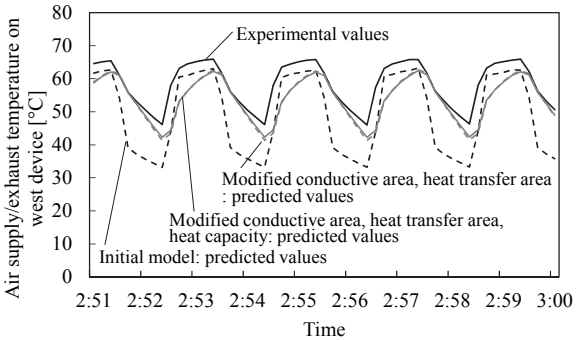

Fig.24: Air supply and exhaust temperatures on west device during final 10 min of experiment.

Heat-recovery efficiency

We calculated the Heat-recovery efficiency η_R when the number of segments of the cylinder was set to 1, 2, 4, 6,

8, 10, and 12 when the flow rate of the fan was set to 20, 35, 55, 60, and 80 m^3/h. Here we define θ_i as the air temperature inside the box, θ_s as the supply air temperature, θ_o as the air temperature outside the box, c_a as the air specific heat of 1,005 J/kg・K, ρ_a as the air density of 1.2 kg/m^3, and q as the flow rate in units of m^3/s. The ventilation thermal load factor η_L is the ratio of the load with heat recovery to that without heat recovery:

$$\eta_L = \frac{c_a \rho_a q(\theta_i - \theta_s)}{c_a \rho_a q(\theta_i - \theta_o)} = \frac{\theta_i - \theta_s}{\theta_i - \theta_o} \quad \text{(Eq.1)}$$

The sum of the thermal load ratio η_L and the heat-recovery efficiency η_R is one, and so η_R is given by

$$\eta_R = 1 - \eta_L = \frac{\theta_s - \theta_o}{\theta_i - \theta_o} \quad \text{(Eq.2)}$$

Because the operation of the devices switches periodically between air supply and exhaust, the procedures for calculating the heat recovery efficiency η_R also involve switching the supply air temperature θ_S and fan flow rates between both devices. *Figure* 25 shows the difference in heat recovery efficiency η_R for different airflow rates for models with different numbers of segmentations. Although the η_R given by Eq.(2) does not depend on the flow rate, because the supply air temperature approaches the temperature of the air outside the box as the flow rate increases, the η_R decreases slightly. The η_R is approximately 0.7 on average.

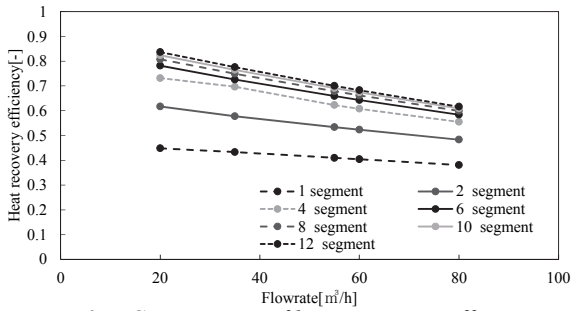

Fig.25: Comparison of heat recovery efficiency.

Three types of thermal load calculation

The current version of NETS has two methods for calculating the thermal load. In the first method, the period for which the temperature is given and the period for which the temperature is solved as an unknown value can be set arbitrarily for any node. In the second method, a manipulation variable is calculated for proportional–integral–differential (PID) control and acts on arbitrary nodes. For example, the heat flow to the circulating water of the floor heating is PID controlled so that the predicted mean vote (PMV) in the room becomes zero (Gotou 2016). The third possible method is an optimum regulator control of a multivariable control system (Owens 1981). The optimal heating/cooling heat flows to multiple circulating water such as in the floor, ceiling piping, and/or coils are solved for so that the core temperature average across multiple human body models becomes 36.8°C (Okuyama 1996).

Conclusion

The concept of this network modeling and NETS can be said to have wide applicability regardless of the spatial dimension, the shape of the object, and the heat transfer form. In the three application cases in this paper, we introduced the possibility of investigating the condensation-prevention and energy-saving effects of an aeration layer inside a wall, the natural ventilation cooling by the chimney effect in a multi-story building, and a heat recovery ventilation device using heat storage and release. The predicted sectional wind speeds for the natural ventilation are close to our measurements experience. The exit temp of the heat recovery device may be improved by the mathematical solution of fluxional calculus.

Acknowledgement

The development of the basic theory of NETS and the computer program was made possible by many previous research studies and the financial support of many companies and universities as well as the Japanese government.

References

Deutinger, C. PASSIV ENERGIE JAPAN, SESERAGHI, Ductless heat recovery ventilation system, HEXAGLOT,Heat strage element Spec., Received Jan. 2013

Gotou, Y. Comparison between one and two dimensional heat transfer models for cross-section of hot water floor heating, Summaries of Graduation thesis of Kanagawa university, 2016, Feb, 95-96

JIS-A2201, Test method for performance of building airtightness by fan pressurization, 2003,p30,4

Lin, K. Shinsuke, K. Study on improvement of double-skin system of room-side air gap applied to detached house - Numerical performance evaluation of natural ventilation and active ventilation in summer and winter (Part1), J. Eng., AIJ, Vol.80, No.713, 583-590, Jul., 2015

Okuyama H. State space approach to building environmental analysis using thermal network Concepts. Shimizu Tech Res Bull Mar.1985;4:45-51.

Okuyama H. Theoretical study on the thermal network model in buildings, Doctorate thesis, Waseda Univ. Dec.1987.

Okuyama H. Optimization Theory for State and Energy Supply Based on a Heat and Moisture Transfer Network Model and Numerical Investigation, Proceedings of the 7th International Conference on Indoor Air Quality and Climate, Nagoya Japan, July 21-26, volume (2), 1996, 485-490

Okuyama H. Thermal and airflow network simulation program NETS. Proceedings of the 6th International IBPSA Conference (Building Simulation'99), Kyoto, Japan; September 1999. pp 1237- 44.

Okuyama H. Verification of Thermal and Airflow Network Model Simulation Program NETS, Technical Papers of Annual Meeting of IBPSA-Japan, Jun. 2002, 15-22

Okuyama H. Onishi Y. System parameter identification theory and uncertainty analysis methods for multi-zone building heat transfer and infiltration, Building and Environment, 54 (2012), 39-52

Owens, D. H. Multivariable and Optimal Systems, Academic Press Inc.(London) Ltd.1981,282-291

SHASE-J, Air Conditioning and Sanitary Engineering Handbook, Fundamentals 1, Feb. 2010, 139 - 153

A TRaNsient SYstems Simulation Program, The University of Wisconsin, https: // sel. me. wisc. edu / trnsys / Jun. 2018